pubs.acs.org/Biomac

Article

Engineered Fluorescent Carbon Dots and G4-G6 PAMAM Dendrimer Nanohybrids for Bioimaging and Gene Delivery

Ivo Martins, Helena Tomás, Fernando Lahoz, and João Rodrigues*

Cite This: *Biomacromolecules* 2021, 22, 2436−2450

Read Online

ACCESS | Metrics & More | Article Recommendations | Supporting Information

ABSTRACT: Carbon dots (CDs) and G4-G6 (polyamidoamine)-PAMAM-NH_2 dendrimers were self-assembled to produce CDs@PAMAM nanohybrids for transfection and bioimaging purposes. CDs were synthesized by the hydrothermal method, using ascorbic acid as a starting precursor and characterized by transmission electron microscopy, UV−Vis, and fluorescence (in solution and solid-state) techniques. CDs were electrostatically combined with PAMAM dendrimers at room temperature, and the UV−Vis, fluorescence, and NMR spectroscopies were used to confirm the self-assembly. When compared to pristine CDs, nanohybrids were more photostable, resisting high acidic and basic pH. Moreover, they were considerably internalized by cells, as assessed by flow cytometry and fluorescence microscopy, and, when excited, displayed multicolor emission easily quantified and visualized. These nanoscale hybrids, coined hybridplexes, can condense pDNA and transfecting cells successfully, particularly the G5 CDs@PAMAM nanohybrids. In summary, CDs prepared in mild and smooth lab conditions, showing good optical properties, were used to prepare elegantly CDs@PAMAM nanohybrids with promising biomedical applications.

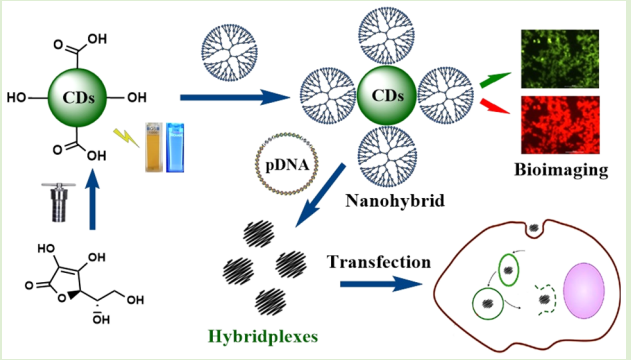

1. INTRODUCTION

With the development of nanoscale materials that exhibit fascinating properties for applications in health and wellness,[1] environmental science,[2] engineering, and industry,[3−5] nanoscience and nanotechnology are at the forefront of modern research. The continuous research in nanoscience and nanotechnology already benefits humanity, and its continuous development will undoubtedly increase its impact in the long term. Among nanomaterials, dendrimers have been intensively studied due to their many potential applications, particularly in the biomedical field.[6−22] These polymeric molecules structured in a dendritic form were first introduced by Vögtle[23] and later designated as "dendrimers" by Tomalia *et al.*[24] Poly(amidoamine) (PAMAM) dendrimers are probably the most widely known dendritic structures. Due to their captivating properties of loading capacity, monodispersity, water solubility, surface functionality, and controlled molecular weight, biomedical applications have been explored, mostly for drug and gene delivery.[25−33] PAMAM dendrimers are interesting for gene delivery due to their excellent DNA condensation properties, forming cationic DNA condensates that interact with the anionic cell surface, significantly increasing cell penetration and efficiently delivering DNA.[34] However, PAMAM dendrimers' cytotoxicity is still a major concern, increasing with the generation and being dependent on the type of terminal groups.[35] For instance, dendrimers containing primary amines at the surface are more toxic than those having secondary or tertiary amines and those with anionic carboxylic groups.[36] Still, the excellent DNA condensation and cell penetration capability are mostly achieved by the PAMAM dendrimers having primary amine termini. Another important limitation of dendrimers when used as bionanomaterials is that they do not present a traceable signal that allows their localization inside cells or the physiological environment. Indeed, although several works revealed that they show intrinsic fluorescence, the intensity of the emitted light is extremely low and in the blue region of the spectrum, thus being shaded by the auto-fluorescence of cells.[37]

Another nanomaterial that has been receiving increased attention since its discovery in 2004 by Xu and co-workers[38] is carbon dots (CDs). Carbon dots are a class of zero-dimensional nanomaterials, mainly composed of carbon, with sizes normally ranging between 2 and 20 nm. Regarding structure, three distinct ones were already reported:[39] the graphene quantum dots (GQDs), carbon quantum dots (CQDs), and carbon nanodots (CNDs). GQDs are well-

Received: February 19, 2021
Revised: April 16, 2021
Published: May 19, 2021

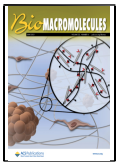

https://doi.org/10.1021/acs.biomac.1c00232
Biomacromolecules 2021, 22, 2436−2450

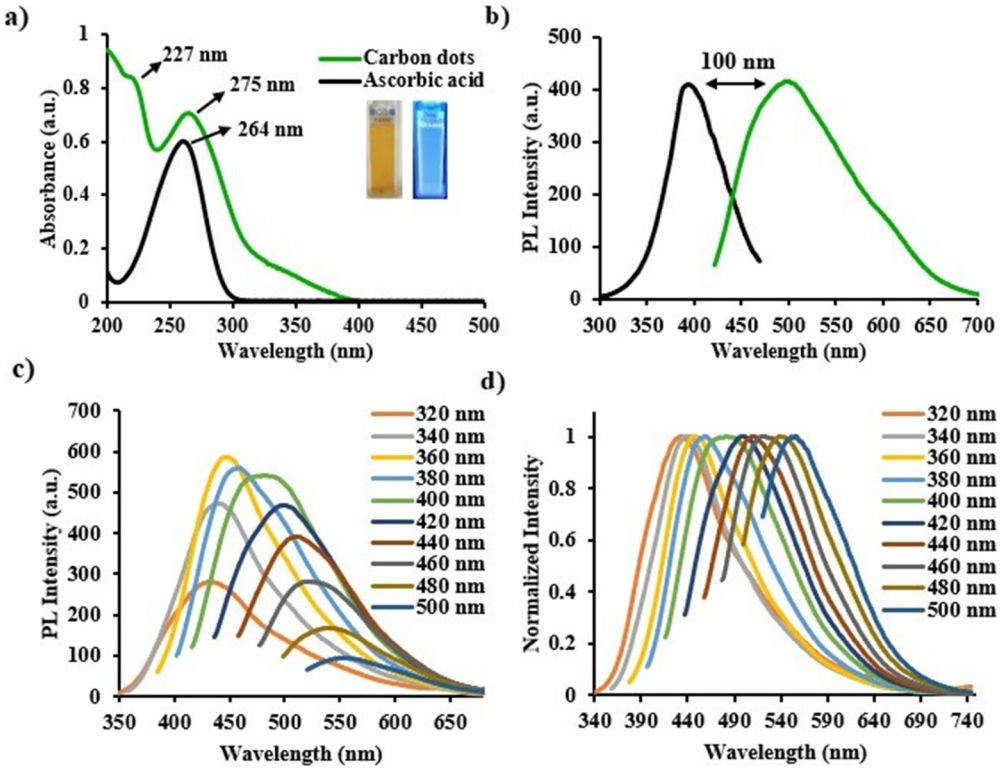

Figure 1. (a) UV−Vis absorption spectra (inset: ambient light/UV light CDs solution images), (b) excitation spectrum for λ_{em} = 500 nm), (c) fluorescence emission spectra, and (d) normalized fluorescence emission spectra of carbon dots in ultrapure water.

defined sp^2 carbon structures, while carbon quantum dots have crystalline sp^2/sp^3 carbon structures, and carbon nanodots have sp^3 carbon cores randomly organized.[39] All these nanomaterials are photoluminescent, of low cytotoxicity, photostable, water-soluble, and biocompatible.[40] Moreover, carbon dots already have an impressive set of potential applications in biomedicine,[41−43] optoelectronics,[44] sensing,[45] and catalysis.[46]

Specifically, the synthesis of carbon nanodots seems interesting since it does not require any additional reaction steps. In general, it is a one-pot synthesis process, and the fluorescent properties are as good as the ones in GQDs and CQDs. Although the fluorescence origin is still a matter of substantial debate and controversy,[39] it is recognized that their surface plays a crucial role in the observed fluorescent properties. The electron-rich surface of carbon dots comes from individual emitters, e.g., small fluorescent entities that act as emission centers, localized in the nanoparticle surface, and highly responsible for their peculiar fluorescence properties.[39] In the last decade, the fluorescence capability of carbon dots has been explored for possible biomedical applications with relative success, especially in combination with polymers.[47−57] In this regard, and as expected, CDs-polymer nanohybrids were shown to be less cytotoxic when neutral polymers were used, such as polyethylene glycol.[49] However, many applications require the use of cationic polymers, as is the case of nucleic acid delivery. In this sense, a few works report the use of poly(ethyleneimine) (PEI) in combination with CDs for both gene and siRNA delivery.[47,48] Being a classical branched polymer, PEI consists of polydisperse molecules that make the hybrids less prompt to be applied in a clinical scenario. Dendrimers, on the contrary, are monodisperse polymers avoiding this handicap. Nanohybrids of CDs and dendrimers have also been prepared based on CDs from different carbon sources and envisaging distinct applications, most of them in the biosensors and drug delivery fields.[50−57] Indeed, a review focused on this subject was very recently published, highlighting the application of this type of nanohybrids in biosensing and cancer theranostics.[58] According to this review and to the best of our knowledge too, to date, only a recent work associated CDs with PAMAM dendrimers having in view gene delivery applications.[57] In that study, CDs were prepared from sweet lemon peel and chemically bonded to low generation dendrimers (G1, G2, and G3) to obtain nanohybrids that were promising as targeted non-viral vectors.

In the present work, engineered CDs@PAMAM nanohybrids were prepared from CDs and activated high generation of PAMAM dendrimers (G4, G5, and G6), and the possibility of their use as gene delivery vectors was evaluated. CDs were prepared from ascorbic acid, which corresponds to a consistent and reliable source of carbon, having in mind the requirements for future clinical application. Ascorbic acid is also among the large universe of organic molecules, an inexpensive source of carbon. Furthermore, the nanohybrids were prepared by direct self-assembly of CDs and dendrimers. This non-covalent approach, in the detriment of covalent bonding, is expected to present some advantages, e.g., lower impact on CDs fluorescence signal and quite-easy experimental setup. In its turn, the choice for high-generation dendrimers was based on their excellent behavior as non-viral transfection agents, especially after being activated by a heating step.[59−61] Although higher generation dendrimers are known to be more cytotoxic due to their high positive charge, their combination with anionic CDs may preclude this problem. Overall, the objective was to take advantage of both

https://doi.org/10.1021/acs.biomac.1c00232
Biomacromolecules 2021, 22, 2436−2450

component properties and obtain novel traceable, cytocompatible, and efficient CDs@PAMAM nanohybrids for gene delivery purposes.

2. EXPERIMENTAL SECTION

2.1. Materials. All chemicals were used as received unless otherwise stated. L-ascorbic acid (purity = 99%) was bought from TCI Chemicals, pyrene was from Sigma-Aldrich, and cyclohexane (NORMAPUR) was purchased from VWR. Thermo Fisher Scientific supplied sodium hydroxide, sodium chloride, potassium chloride, and hydrochloride acid (37%). Riedel-de-Haën supplied potassium dihydrogen phosphate, while boric acid (AnalaR) was purchased from BDH. Citric acid and diethyl barbituric acid were bought from Merck. Ethylenediamine core PAMAM dendrimers G4 (MW 14215 Da, 64 NH_2 terminal groups), G5 (MW 28826 Da, 128 NH_2 terminal groups), and G6 (MW 58048 Da, 256 NH_2 terminal groups) in methanol were purchased from Dendritech Inc. The cellulose ester dialysis membrane (MWCO 100−500 Da) was purchased from SpectraLabs. Dulbecco's modified Eagle's medium (DMEM), fetal bovine serum (FBS), phosphate-buffered saline (PBS) solution, trypsin solution (0.25 w/v), and antibiotic-antimycotic solution 100x (AA, containing amphotericin B, penicillin, and streptomycin) were purchased from Life Technologies, while trypan blue, resazurin, and the plasmid DNA purification kit were bought from Sigma-Aldrich. The cell lysis buffer and the Quant-iT PicoGreen dsDNA assay kit were purchased from Thermo Fisher Scientific. The luciferase and bicinchoninic acid assay kits were from Promega and Sigma-Aldrich, respectively. Cell culture dishes were from VWR. Ultrapure water (UPW) used throughout the experiments was filtered by a Millipore Milli-Q direct water purification system and presented a resistivity higher than 18.2 MΩ·cm.

2.2. Synthesis of Carbon Dots. Carbon dots were synthesized using ascorbic acid as the starting material. Briefly, 500 mg of ascorbic acid was dissolved in 10 mL of UPW, the transparent solution was then inserted in a 100 mL stainless steel Teflon container, and the reaction took place in an oil bath at 200 °C for 5 h. Afterward, the obtained black solution was dialyzed against UPW for 72 h using a 100−500 Da dialysis membrane and centrifuged at 10000 rpm for 10 min to remove the insoluble particles. The purified CDs solution was stored sheltered from light at room temperature, and a part was freeze-dried for further tests and characterization.

2.3. Self-Assembly of G4-G6 CDs@PAMAM Nanohybrids. Dendrimers solutions were first lyophilized to remove the methanol. Before the self-assembly process, the G4-G6 PAMAM-NH_2 dendrimers were activated by heating the solutions in a water bath at 40 °C for 24 h.[61] Typically, 2.5 mL of 4 mg mL^{-1} aqueous CDs solution was mixed with 5 mL of 8 mg mL^{-1} G4-G6 PAMAM-NH_2 dendrimers, and 2.5 mL of UPW was added to complete a 10 mL final volume. The reactions were carried at room temperature under stirring conditions for 24 h and sheltered from light to produce CDs@PAMAM hybrids. Then, the solutions of G4-G6 CDs@PAMAM hybrids were freeze-dried for mass concentration determination and further characterization.

2.4. Characterization of CDs/CDs@PAMAM Nanohybrids. *2.4.1. UV−Vis Spectroscopy.* The UV−Vis absorption spectra were obtained using a UV−Vis spectrophotometer (Lambda 25) from PerkinElmer and 1 cm light path quartz cuvettes. Ultrapure water was used as the solvent. The concentration used to obtain the UV−Vis absorption spectra of ascorbic acid and CDs (Figure 1a) was 50 μg mL^{-1}. As for the UV−Vis absorption of G4-G6 CDs@PAMAM hybrids and respective CDs (Figure 4a), the concentration was 20 μg mL^{-1}.

2.4.2. Fluorescence Spectroscopy. Photoluminescence (PL) spectra were collected using a fluorescence spectrometer (LS55) from PerkinElmer. The range of excitation wavelengths used was 320−500 nm with 20 nm increments. Excitation and emission slits were 10 and 8 nm, respectively. The scan speed was set at 500 nm/min, and 1 cm light path quartz cuvettes were used in all the measurements. The excitation and photoluminescence spectra of CDs (Figure 1b,c) were obtained using a 1 mg mL^{-1} concentration. Regarding the PL spectra of G4-G6 CDs@PAMAM hybrids, the concentration used was 200 μg mL^{-1}, and for CDs, 40 μg mL^{-1} (comparison purposes), obtained using a fixed 360 nm excitation (Figure 4b). Moreover, all emission spectra were collected using the same experimental conditions.

2.4.3. Fluorescence Lifetime Measurements in the Solid State. The fluorescence lifetime of CDs was measured using a 375 nm picosecond pulsed diode laser (Edinburgh Instruments EPL-375), with a typical pulse width of 80 ps, and recorded using a zero temporal dispersion fluorescence spectrometer equipped with a single photon counting multichannel plate photomultiplier and dedicated acquisition software (Edinburgh Instruments LifeSpec II and F900 software).

2.4.4. Fourier Transform Infrared Spectroscopy (FTIR). The surface functionalities of CDs and G4-G6 CDs@PAMAM hybrids were analyzed using an FTIR (Spectrum Two FTIR spectrometer) from PerkinElmer coupled to an ATR (attenuated total reflectance) accessory (DuraSampl*IR* II) from Smiths Detection. The raw materials were studied in the solid state, and the light detected after reflectance respected a minimum of 14%; the spectra were collected using a wavenumber range of 650−4000 cm^{-1}.

2.4.5. Nuclear Magnetic Resonance (NMR) Spectroscopy. The NMR spectra were obtained using a 400 MHz NMR (UltraShield 400 plus ULTRA LONG HOLD) equipment from Bruker. Briefly, ca. 10 mg of the sample was dissolved in 540 μL of deuterated oxide or DMSO-d_6. The ^{13}C and ^{1}H NMR spectra were used to monitor the differences before and after synthesis/self-assembly of carbon dots/G4-G6 CDs@PAMAM hybrids as well as to identify their surface functional groups.

2.4.6. Transmission Electron Microscopy (TEM). The morphology of carbon dots and G4-G6 CDs@PAMAM nanohybrids was obtained using a Hitachi 8100 TEM instrument with digital image acquisition and a 200 kV acceleration voltage (Marked Grids, 50 mesh, 3.0 mm O.D., Copper).

2.4.7. Dynamic Light Scattering (DLS) and ζ-Potential Measurements. Information on hydrodynamic diameter and ζ-potential was obtained using a Zetasizer Nano ZS equipment from Malvern Instruments equipped with a He-Ne laser with a 633 nm wavelength. The hydrodynamic diameter determination assays were made using a standard polystyrene cuvette, employing UPW in the dilutions. The samples were previously filtered with a 0.22 μm filter, and the analysis was carried out at 25 °C using 10 runs/10 s; results shown are from three independent measurements. The ζ-potential measurements were made using a polystyrene capillary cell, and the data were analyzed after 20 runs; three independent measurements were also performed. The concentration used in the DLS measurements for CDs, hybrids, and dendrimers was 250 μg mL^{-1}.

2.4.8. Quantum Yield Evaluation. The quantum yield was determined using the slope method and pyrene (Q_y = 32%) as the fluorescence standard. Briefly, pyrene in cyclohexane and carbon dots in UPW were prepared to have absorbances between 0.01 and 0.1 (five samples of each were used). The absorbance and PL spectra were obtained by UV−Vis and fluorescence spectroscopies (λ_{ex} = 317 nm), respectively. The integrated emission spectrum values were obtained using the FL WinLab software from PerkinElmer, and the integrated emission spectra against the absorbance of pyrene and carbon dots' solutions were plotted. The fluorescence quantum yield was obtained using the slope method (eq 1): Q_{yR} is quantum yield of the reference molecule, m is the slope of the line, n is the refraction index of the solvent used, and R denotes the values for the used reference.

$$Q_y = Q_{yR}(m/m_R) \times (n^2/n^2R) \quad (1)$$

2.4.9. Effect of pH and Ionic Strength on Fluorescence Intensity. The effect of pH and ionic strength conditions on the fluorescence intensity of CDs and G4-G6 CDs@PAMAM nanohybrids was evaluated. The pH was measured using a pH meter model 3510 from Jenway. The studies at different pH values were performed using

https://doi.org/10.1021/acs.biomac.1c00232
Biomacromolecules 2021, 22, 2436−2450

Scheme 1. Representation of the (a) Hydrothermal Synthesis of Anionic Carbon Dots and (b) Their Self-Assembly with PAMAM Dendrimers (Generations 4 to 6) through Electrostatic Interactions to Produce G4-G6 CDs@PAMAM Nanohybrids

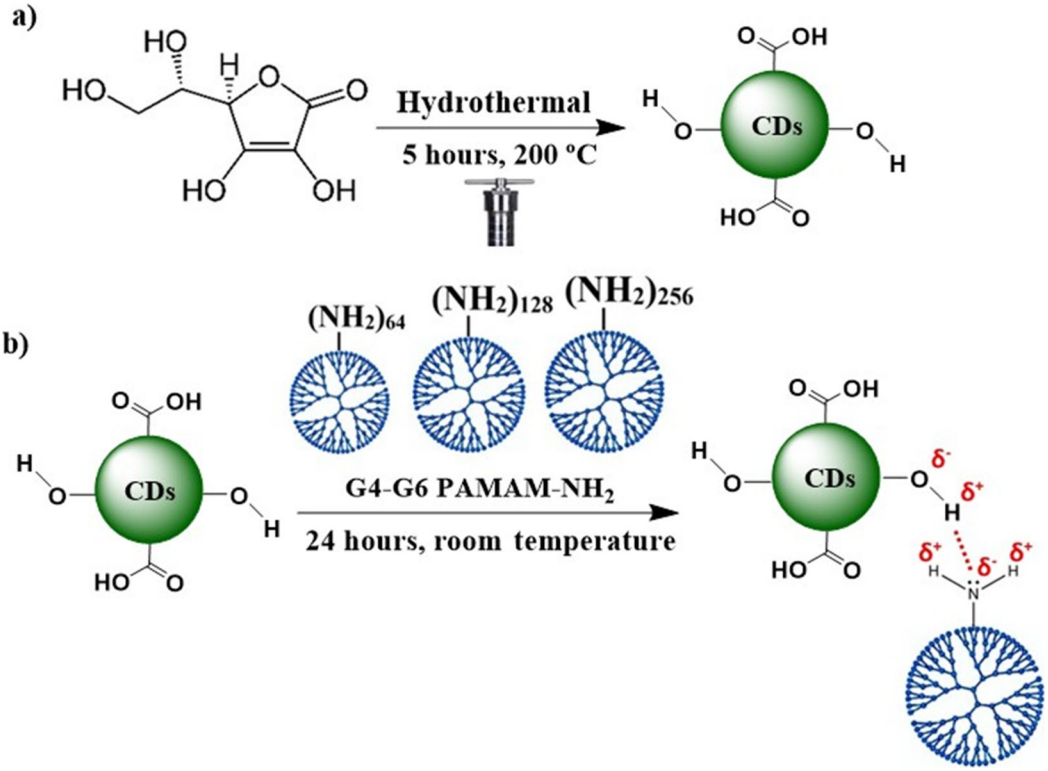

a pH range of 1−14 as follows: 250 μL of a solution containing G4-G6 CDs@PAMAM nanohybrids at a concentration of 0.8 mg mL^{-1} and CDs at 0.2 mg mL^{-1} was added to 750 μL of a universal buffer solution at a set pH value (the buffer composition comprised 6 g of citric acid, 3.9 g of monopotassium phosphate, 1.8 g of boric acid, and 5.3 g of diethylbarbituric acid dissolved in 1 L of UPW; the pH of the buffer was adjusted to the desired value with HCl or NaOH 1 M solutions). The studies at different ionic strengths were made using NaCl and KCl as ionic strength agents within a concentration range of 0−200 mM (20 mM increments). Again, 250 μL of a solution containing carbon dots or G4-G6 CDs@PAMAM nanohybrids at a concentration of 0.2 mg mL^{-1} was placed in a 1.5 mL vial. Then, 750 μL of another solution containing the ionic strength agent at an appropriate molar concentration was placed in the vial (the final concentration of carbon dots or G4-G6 CDs@PAMAM nanohybrids was 50 μg mL^{-1}). In the end, for both cases, 100 μL of the final solutions was added in quadruplicate to a white 96-well plate, and the fluorescence was read using a microplate reader (PerkinElmer VICTOR^3 1420) and an excitation wavelength of 345 nm.

2.5. Biological Studies. *2.5.1. Cell Viability Evaluation.* HEK 293T cells were seeded at 5000 cells/well in 96-well plates and allowed to incubate for 24 h at 37 °C in a 5% CO_2 humidified atmosphere. The cells were cultured in DMEM supplemented with 10% (v/v) FBS and 1% (v/v) AA 100x solution. Afterward, cells were exposed to CDs, G4-G6 CDs@PAMAM hybrids, or pristine G4-G6 PAMAM dendrimers dissolved in a supplemented cell culture medium at concentrations of 1, 10, 25, 50, and 100 μg mL^{-1} (quadruplicate) for 48 h. After, the culture medium was removed, and cells were washed twice with PBS. Then, 100 μL of fresh culture medium was placed in each well followed by the addition of 100 μL of resazurin solution (0.1% w/v in PBS). Cells were then allowed to incubate again for 3 h, and, after this period, 100 μL from each well was transferred to a white 96-well culture plate for resorufin fluorescence quantification (λ_{ex} = 530 nm, λ_{em} = 590 nm) in a microplate reader (PerkinElmer VICTOR^3 1420). Results are presented as a percentage of the fluorescence intensity value obtained for non-exposed cells.

2.5.2. Cellular Internalization Assays. The cellular internalization of CDs and G4-G6 CDs@PAMAM hybrids was conducted using HEK 293T cells and the flow cytometry technique. The cells were seeded in 24-well culture plates at 1.5 × 10^5 cells per well for 24 h and incubated at 37 °C and in a 5% CO_2 humidified atmosphere. Subsequently, cells were exposed to 300 μg mL^{-1} CDs and G4-G6 CDs@PAMAM hybrids for a 24 h incubation time. Then, the cell culture medium was removed, cells were washed twice with PBS, detached using a 0.25% (w/v) trypsin solution, and analyzed by flow cytometry, recording a minimum of 10,000 events. The excitation laser had 405 nm, and the measurements were performed using two different detection channels, AmCyan (530 nm) and Qdot 605 (615 nm), in an ACEA-NovoCyte 3000 flow cytometer equipment. The presence of CDs and G4-G6 CDs@PAMAM hybrids inside HEK 293T cells was also observed by fluorescence microscopy. HEK 293T cells were seeded in 48-well culture plates at 5 × 10^4 cells/well and incubated for 24 h at 37 °C and in a 5% CO_2 humidified atmosphere. Then, 300 μg mL^{-1} CDs and G4-G6 hybrids were exposed to cells for a 24 h incubation time, and samples were observed using an inverted fluorescence microscope TE2000-E from Nikon. The excitation filters used were 450−490 and 510−560 nm to obtain green and orange/red fluorescent cells, respectively.

2.5.3. DNA Condensation Assays. A plasmid DNA (pDNA) encoding enhanced green fluorescent protein and luciferase genes (pEGFPLuc, 6.4 kb) was amplified in *Escherichia coli* that was grown overnight in Luria-Broth medium containing antibiotic. The plasmids were then extracted and purified using the GenElute Endotoxin-free Maxiprep Plasmid Purification Kit following the manufacturer's instructions. A small amount of plasmid was dissolved in UPW, and the absorbance was read at 260 and 280 nm to evaluate its purity and amount produced. The capacity of CDs, G4-G6 CDs@PAMAM hybrids, and pristine G4-G6 PAMAM dendrimers to condense pDNA was then studied using the PicoGreen assay. Condensates formed with pDNA were prepared at different CD/pDNA, nanohybrid/pDNA, or dendrimer/pDNA weight ratios, namely, 1, 2, 5, 10, 20, 50, and 100. Briefly, in the preparation of hybridplexes, 10 μL of a 150 μg/mL solution of plasmid DNA (pDNA) was added to each vial

https://doi.org/10.1021/acs.biomac.1c00232
Biomacromolecules 2021, 22, 2436−2450

followed by the addition of the needed volume of solution containing the CDs, G4-G6 CDs@PAMAM hybrids, or pristine G4-G6 PAMAM dendrimers to prepare condensates at the set ratios. Then, using Tris-EDTA (TE) buffer (pH 8.0, present in the kit), the solution was completed to 1 mL of the final volume. The final content of pDNA in each vial was 1.5 μg. The solutions were then mixed in the vortex and allowed to incubate for 20 min at room temperature. Subsequently, 100 μL of each solution was transferred to white 96-well plates (quadruplicate), and 100 μL of a diluted PicoGreen solution (200x dilution) was added to each well followed by incubation at room temperature for 5 min, protected from light. The PicoGreen fluorescence was read in a microplate reader (PerkinElmer, model VICTOR^3 1420, λ_{ex} = 485 nm, λ_{em} = 535 nm). The blank solution was composed of 100 μL of PBS mixed with 100 μL of PicoGreen.

2.5.4. Transfection Assays. HEK 293T cells were seeded in a 24-well culture plate at 2×10^4 cells/well and incubated for 24 h at 37 °C and in a 5% CO_2 humidified atmosphere. Then, CDs/pDNA, G4-G6 CDs@PAMAM/pDNA, and G4-G6 PAMAM/pDNA condensates at weight ratios of 2, 10, and 20 were placed in the respective wells at a final content of pDNA of 1.5 μg per well. A supplemented cell culture medium containing FBS was then added to the wells, and cells were left inside the incubator. Non-transfected cells and cells transfected with naked pDNA were used as negative controls. Forty-eight hours post-transfection, cells were observed in an inverted fluorescence microscope (TE2000-E from Nikon) to detect GFP expression. Later, the cell culture medium was removed, and the cells washed twice with PBS and added 100 μL of lysis buffer to release their content. The total content in protein and luciferase activity was then quantified in each well using the bicinchoninic acid kit (absorbance was read at 562 nm) and the luciferase assay kit, respectively, following the supplier's instructions. Luminescence intensity was quantified using a microplate reader (PerkinElmer, model Victor^3 1420) set for a 3 s delay with signal integration for 10 s. The luciferase activity results were normalized with respect to the total protein content and expressed as relative light units (RLU) per mg of protein.

2.6. Statistical Analysis. The results obtained are presented as mean ± standard deviation (StDev), and the data were analyzed using the Student's *t*-test to evaluate the statistical significance, and the *p*-values used are represented as *($p < 0.05$), **($p < 0.01$), and ***($p < 0.001$).

3. RESULTS AND DISCUSSION

3.1. Synthesis and Characterization of Carbon Dots. The first step of the present work was to synthesize CDs from ascorbic acid using a hydrothermal process (Scheme 1a). Beyond the advantages mentioned before, ascorbic acid is an interesting precursor for the synthesis since the chemical groups present in this molecule, namely, those containing oxygen, can result in CDs having unique properties. The use of ascorbic acid was previously considered for CDs synthesis by others using high temperatures and different reaction times, either in combination with other organic molecules or using it from natural extracts.[62−65] In our case, the synthesis of carbon dots was carried out using only ascorbic acid as the reaction precursor and milder reaction conditions that were original and optimized. Namely, 200 °C and a 5 h reaction time were applied in a stainless steel Teflon container inside an oil bath. During the synthesis, ascorbic acid experienced degradation, forming new structures and chemical groups, generating small oxygen-rich fluorescent molecules. Part of the fluorescent molecules was carbonized to generate carbon cores, and the remaining were chemically bonded, forming the fluorescent carbon dots. The black solution containing CDs was subjected to dialysis for 3 days to remove free small fluorescent molecules generated during the process and centrifuged to isolate the insoluble particles from the CDs solution (yield of 10%).

The photophysical properties of carbon dots were evaluated and are shown in Figure 1, which comprises their UV−Vis absorption spectrum and their excitation and emission fluorescence spectra, including normalized fluorescence emission spectra. The UV−Vis spectrum of ascorbic acid (Figure 1a) presents its typical absorption band centered at 264 nm due to $\pi-\pi^*$ (C═C) transitions. The CDs exhibit two characteristic absorption bands: one shoulder at 227 nm and a maximum at 275 nm assigned to $\pi-\pi^*$ (C═C) and $n-\pi^*$ (C═O, conjugated system) transitions. CDs' solutions at ambient light show a typical light brown color and, after UV excitation, the characteristic blue color of the dots (inset in Figure 1a). An excitation spectrum was registered using an emission wavelength of 500 nm (Figure 1b). The resulting excitation band's position concerning the emission wavelength shows a large Stokes shift of around 100 nm. The prepared CDs' fluorescence emission spectra were obtained employing excitation wavelengths between 320 and 500 nm with 20 nm increments (Figure 1c). These spectra displayed red shifts in the maximum emission wavelength accompanied by fluorescence emission intensity reductions upon increasing the excitation wavelengths. The CDs have shown their strongest fluorescence in the blue region of the visible spectra. More importantly, the normalized intensity spectra (Figure 1d) clearly show that these CDs can emit either in the blue, green, or orange/red region of the visible spectra.

Moreover, the quantum yield of the prepared CDs, determined using the slope method,[66] was 20.0%, a value higher than the obtained by Cailotto *et al.* for CDs also obtained by using ascorbic acid as a precursor (QY of 1.5% calculated using as standard quinine sulfate)[62] (Figure S1 and Table S1 in the Supporting Information).

Photoluminescence studies were further performed with CDs in powder form. The fluorescence decay of CDs solid powder was measured using a high repetition rate UV diode laser at 375 nm. The detection wavelength was tuned at the maximum of the emission band, around 455 nm. The obtained fluorescence decay is given in Figure 2, together with the instrumental response function (IRF) of the experimental setup. The fluorescence decay of CDs showed a non-exponential behavior, which can be expected for CDs that present a very broad emission band due to the superposition of several emissions from diverse emitter centers.[39] In order to quantify the average lifetime value of the fluorescence, the

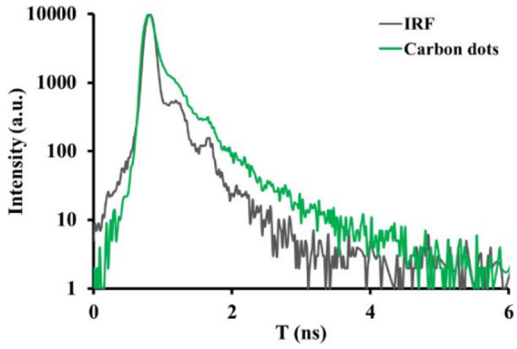

Figure 2. Decay of the fluorescence of CDs measured at 455 nm upon excitation at 375 nm (IRF: instrumental response function). The average lifetime of CDs fitting to a third exponential decay was 0.10 ns.

https://doi.org/10.1021/acs.biomac.1c00232
Biomacromolecules 2021, 22, 2436−2450

decay curves have been successfully fitted to a three exponential decay curve of the type.

$$I(t) = A_1 e^{-t/\tau_1} + A_2 e^{-t/\tau_2} + A_3 e^{-t/\tau_3} \quad (2)$$

where A1, A2, and A3 are the pre-exponential factors, and τ_1, τ_2, and τ_3 are the decay constants. The fitting was made using IRF reconvolution analysis with FAST (Fluorescence Analysis Software Technology) by Edinburgh Instruments.

The average lifetime was then calculated using the following equation:[67]

$$\langle \tau_{av} \rangle = \frac{A_1\tau_1^2 + A_2\tau_2^2 + A_3\tau_3^2}{A_1\tau_1 + A_2\tau_2 + A_3\tau_3} \quad (3)$$

The obtained average lifetime of the CDs excited state was about 0.1 ns (Figure 2). The average lifetime value obtained in the solid samples was notably shorter than those reported for CDs dispersed in water solutions[68,69] and was similar to those reported in CDs solid forms, in which aggregates are formed, and energy transfer processes compete with the radiative transition and nonradiative transition paths, leading to shorter average lifetimes.[70]

Transmission electron microscopy was used to confirm the presence of CDs and to observe their morphology. The obtained results are presented in Figure 3, which shows a TEM micrograph of the CDs with its respective size distribution (see also Figure S2 in the Supporting Information). The results show carbon dots with an apparent round shape and an average size of around 4 nm.

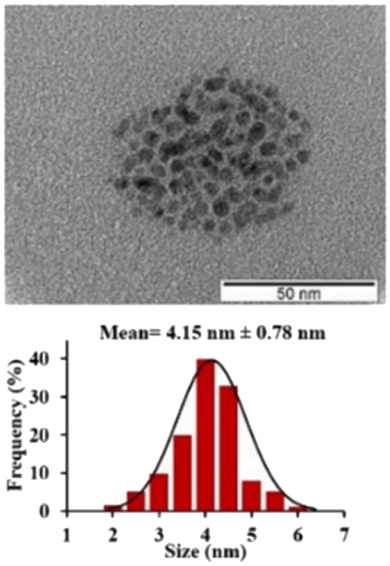

Figure 3. TEM images of carbon dots and their average size distribution.

In addition, carbon dots were characterized by NMR spectroscopy to evaluate the differences between ascorbic acid and the obtained CDs before and after synthesis as well as to identify the chemical groups likely existent at their surface. ^{1}H NMR and ^{13}C NMR spectra of ascorbic acid and carbon dots were recorded in DMSO-d_6. The results are shown in Figures S3 and S4 (in the Supporting Information). The precursor (ascorbic acid) presents its typical signals in both ^{1}H and ^{13}C NMR spectra, which can be easily attributed to each of the hydrogen and carbon atoms, respectively, in the molecular structure. As for the ^{1}H NMR spectra of carbon dots (Figure S3), signals at chemical shifts of 9.2/9.4, 10.3, and 12.4 ppm may be ascribed to different surface functional groups such as aldehyde, alcohols, and carboxylic groups, respectively. The signals at chemical shifts of 5.6 and 6.9/7.1 ppm are assigned to protons bonded to sp^2 carbon and aromatic ring structures, respectively, whereas signals with chemical shifts between 3 and 4 ppm are from protons near carbon-heteroatom groups. Lastly, the signal at a chemical shift of 1.3 ppm is attributed to protons bonded to a sp^3 carbon. The ^{13}C NMR spectrum of CDs (Figure S4 in the Supporting Information) shows a signal at a chemical shift of 30 ppm assigned to alkyl carbons and several other signals at chemical shifts between 60 and 80 ppm that are ascribed to carbons in C−O, C−OH, and C—C═O groups.

The aromatic and sp^2 carbons are assigned to the signals at chemical shifts from 120 to 150 ppm. The signal at the chemical shift of 175 ppm corresponds to carbon in carboxylic groups. The infrared spectrum of the produced CDs was also obtained to identify the different surface functionalities (Figure S5 in the Supporting Information). Ascorbic acid exhibits its typical absorption bands with the most relevant signals at 1024 cm^{-1}, attributable to the C−O group, at 1750 cm^{-1}, assigned to the stretching vibration of C═O, and three sharp bands between 3308 and 3524 cm^{-1} ascribed to structural −OH groups, free −OH from hydrogen bonding, and dimer formation. In the case of carbon dots, the infrared spectrum shows a broad band centered at 3360 cm^{-1} assigned to −OH groups and a stretching vibration at 1707 cm^{-1} assigned to the C═O from the carboxylic group. Bands at 1188 and 1021 cm^{-1} were attributed to C−O−C and C−O groups, respectively.

In summary, based on these results, pure fluorescent carbon dots with an oxygen-rich surface having different functional groups, such as carboxylic and different types of alcohol groups, with an average size of 4 nm and emitting in the blue, green, or orange/red region of the visible spectra, with the optimum excitation wavelength in between 360 and 400 nm, and the strongest emission occurring amid 450−500 nm (blue or light blue), were successfully synthesized.

3.2. Self-Assembly of CDs@PAMAM Nanohybrids.

The prepared carbon dots were self-assembled with G4-G6 PAMAM-NH$_2$ dendrimers to form G4-G6 CDs@PAMAM nanohybrids (Scheme 1b). The process was made by mixing carbon dots and G4-G6 PAMAM-NH$_2$ dendrimers at a 1:4 mass ratio, and the reaction occurred at room temperature for 24 h and under stirring conditions. The dendrimers activation was previously done using a heat treatment since it is reported to improve their action as gene delivery agents.[59−61] The interaction between carbon dots and PAMAM dendrimers is dependent on the nature of the surface groups and takes advantage of the anionic surface of carbon dots to interact electrostatically with the cationic surface of the PAMAM-NH$_2$ dendrimers.

The CDs@PAMAM nanohybrids characterization by UV−Vis and fluorescence spectroscopies was also performed, and the obtained spectra are presented in Figure 4.

As discussed in the previous section, the UV−Vis absorption spectrum of carbon dots has two absorption bands with maximum wavelengths at 227 and 275 nm. After self-assembly with G4-G6 PAMAM-NH$_2$ dendrimers to form the nanohybrids, all spectra presented an absorption band at 279 nm, characteristic of the PAMAM dendrimers structure (Figure

https://doi.org/10.1021/acs.biomac.1c00232
Biomacromolecules 2021, 22, 2436−2450

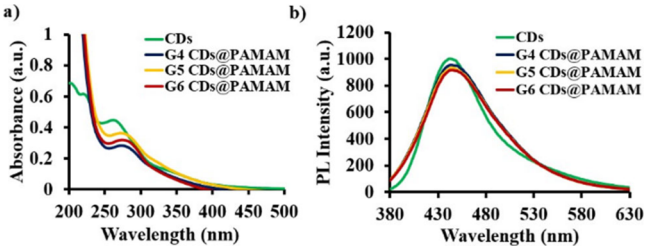

Figure 4. (a) UV−Vis absorption and (b) fluorescence emission (λ_{ex} = 360 nm) spectra of CDs and G4-G6 CDs@PAMAM nanohybrids obtained in ultrapure water. The fluorescence emission spectra were obtained using G4-G6 hybrids with a fixed 200 μg mL^{-1} concentration and the respective CDs at 40 μg mL^{-1}.

4a).[71] This band presence in all nanohybrid spectra absorption suggests that the dendrimer will be most probably surrounding the carbon dots. The emission spectra of carbon dots and G4-G6 CDs@PAMAM nanohybrids were obtained using a fixed 360 nm excitation wavelength. Since the G4-G6 CDs@PAMAM hybrids contain 20% CDs, the pristine CDs concentration was leveled at 40 μg mL^{-1} for comparison purposes. The obtained results (Figure 4b) have shown that the dendrimers had a slight quenching effect over the CDs fluorescence. Depending on the dendrimer generations, a slight 3 nm red shift was also observed, clearly confirming the establishment of interactions between both structures as previously reported by Shi *et al.*[55] Furthermore, the quantum yield was also determined for the G4-G6 CDs@PAMAM nanohybrids, being evident that their formation decreased the fluorescence quantum yield significantly when compared with the CDs. Quantum yield values were 11.9, 10.5, and 7.72% for the G4, G5, and G6-based nanohybrids, respectively (Figure S1 and Table S1 in the Supporting Information) vs 20.0% for new CDs. This observed fluorescence quantum yield reduction also suggests a strong interaction between the CDs and PAMAM dendrimers.

The nanohybrids, along with their respective G4-G6 PAMAM-NH_2 dendrimer and carbon dots, were further characterized by NMR. Since DMSO interferes with the PAMAM dendrimer signals due to its characteristic peak at a chemical shift of 2.5 ppm, all spectra were obtained using D_2O as the deuterated solvent instead of DMSO-d_6. The ^{1}H NMR spectra of G4-G6 PAMAM-NH_2 dendrimers are very similar among them (see also Figures S6−S8 in the Supporting Information for all generations), showing characteristic signals attributable to the different $-CH_2$ groups in the dendrimer scaffold. As for the ^{1}H NMR of carbon dots, it was made in D_2O for comparison with the hybrids and respective pristine PAMAM dendrimers. The signals at chemical shifts of 5.7 and 7.1−7.3 ppm can be assigned to protons bonded to sp^2 carbon and aromatic ring structures, respectively. Moreover, signals at chemical shifts of 3.5−4.5 ppm are due to protons near the heterogroups (such as C−O and C−CO). The signals at chemical shifts of 1−2.6 ppm arise from protons bonded to sp^3 carbon. The protons from the surface functional groups, the aldehyde, alcohol, and carboxyl (at chemical shifts of 9−12 ppm, Figure S6), disappeared due to protonation by D_2O. After self-assembly of CDs with PAMAM dendrimers, the NMR spectra are dominated by the dendrimers' signals. Slight shifts in these signals were observed in relation to those present in pristine dendrimers' spectra, indicating the occurrence of interaction and the formation of the expected nanohybrids.

The infrared spectra of CDs and G4-G6 CDs@PAMAM hybrids were also obtained (Figure S9 in the Supporting Information), and, as previously discussed, the IR spectrum of carbon dots indicated a surface rich in carboxylic and hydroxylic groups. After interaction with the PAMAM dendrimers to form G4-G6 nanohybrids, a stretching vibration band at 3260 cm^{-1} was obtained and ascribed to the amine groups of the PAMAM structure. Furthermore, bands at 1627 cm^{-1} corresponded to the stretching C═O of amides and, at 1544 cm^{-1}, to the N−H bending mode. Overall, the FTIR results show, as expected, the prevalence of the PAMAM dendrimer absorption bands.

The morphology of the G4-G6 CDs@PAMAM nanohybrids was also evaluated by TEM, as presented in Figure 5. The

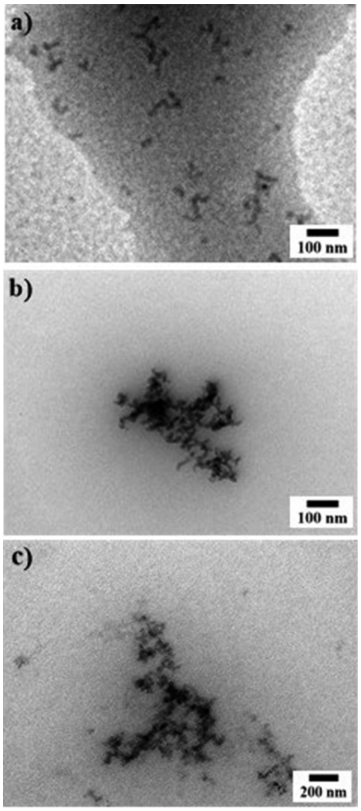

Figure 5. TEM micrographs of (a) G4-based, (b) G5-based, and (c) G6-based CDs@PAMAM nanohybrids. Scale bars: 100 nm in (a) and (b); 200 nm in (c).

micrographs show amorphous G4-G6 CDs@PAMAM nanohybrids with the dark and grey regions corresponding to agglomerated carbon dots and the surrounding PAMAM dendrimers, respectively. Due to its small size and fragile organic composition, the PAMAM dendrimer structure is very sensitive to the microscope electron-beam. As so, its observation is difficult to be achieved.[72] However, the self-assembly of CDs with dendrimers forms a dark condensed structure with no need to use contrast agents or staining methods to visualize all the hybrids.

The hydrodynamic diameter of CDs and G4-G6 CDs@PAMAM nanohybrids was determined by dynamic light scattering. The obtained results are shown in Figure S10 in the Supporting Information. The average hydrodynamic

https://doi.org/10.1021/acs.biomac.1c00232
Biomacromolecules 2021, 22, 2436−2450

diameter of carbon dots was around 9 nm, whereas those for G4-G6 CDs@PAMAM nanohybrids ranged between 20 and 40 nm. The ς-potential was measured as well (Table S2 in the Supporting Information). The ς-potential of the prepared carbon dots is -5.72 ± 0.62 mV, corresponding to an anionic surface particle. The ς-potential values of the G4-G6 PAMAM-NH_2 dendrimers were 2.72 ± 0.56, 5.93 ± 1.15, and 8.89 ± 1.29 mV. The formed G4-G6 CDs@PAMAM nanohybrids presented ς-potentials of -0.414 ± 0.50, -0.765 ± 0.31, and $+1.63 \pm 0.29$ mV, respectively. This increase in the ς-potential when compared with the free CDs confirms the self-assembly with the positively charged PAMAM dendrimers.

In summary, results from photoluminescence, ^{1}H NMR, FTIR, TEM, DLS, and ς-potential measurement techniques indicate that fluorescent G4-G6 CDs@PAMAM nanohybrids were successfully prepared, having average hydrodynamic diameters between 20 and 40 nm. Moreover, the quenching of fluorescence after self-assembly, the prevalence of the absorption bands from the dendrimers observed in the UV and FTIR spectroscopy characterization, as well as the dominance of ^{1}H NMR signals from the PAMAM dendrimers in the correspondent nanohybrids spectra, confirms that nanohybrids are formed by CDs surrounded by a shell of dendrimers.

3.3. Effect of pH and Ionic Strength on G4-G6 CDs@PAMAM Nanohybrids Fluorescence Intensity. In nanomedicine applications, pH is an important parameter to consider since it may substantially change during the nanomaterial path toward the biological target. Unless the idea is to use the nanomaterial as a probe for pH determination, the fluorescence intensity should be maintained at high enough levels for its effective tracing in the biological system. In this regard, the pH effect on the fluorescence intensity of CDs and G4-G6 CDs@PAMAM nanohybrids was evaluated (Figure 6 and Figure S11 in the Supporting Information). In these experiments, a universal pH buffer was used (constant composition), and fluorescence intensity was measured by adjusting the pH to the desired value.

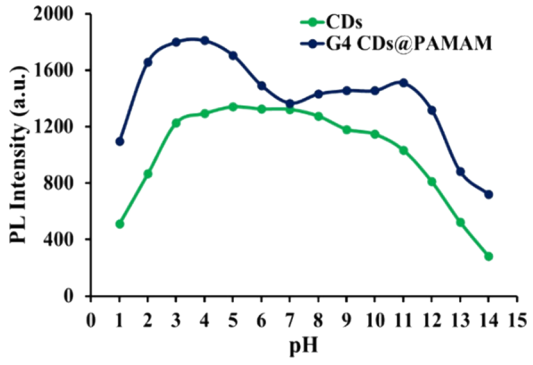

Figure 6. Effect of pH on the fluorescence intensity of CDs and G4 CDs@PAMAM nanohybrids.

The results obtained for carbon dots show that the fluorescence drops 50−60% at strong acid and basic environments, almost reaching a plateau between pH 3 and 8. As for the G4-G6 CDs@PAMAM nanohybrids, their fluorescence intensity does not present this behavior, and, on the contrary, fluorescence emission has maxima at pH values between 3 and 4. The fluorescence drops and reaches near the same PL intensity at neutral pH values compared to pristine CDs, increasing their fluorescence intensity between pH 10 and 11. In fact, we can consider that the self-assembly of the CDs with the dendrimers results in nanohybrids that globally present a higher fluorescence intensity in all pH ranges, making them better nanomaterials for bioimaging purposes. Likely, PAMAM dendrimers protect the emission centers present in CDs from high and low H^+ concentrations. If we consider that CDs have different emission centers, some of which can be affected at low pH values, others at high pH values, then it is clear that dendrimers' presence protects these emission centers from the surrounding environment. In fact, dendrimers can act as proton sponges, a feature that has been reported in the literature and that is partly responsible for their good behavior as vehicles for the delivery of nucleic acids. Here, it is likely that the dendrimers, also acting as proton sponges, decrease the acidic environment around the CDs at low pH values. On the other hand, at high pH values, dendrimers can release the protons immobilized in their structure, thus reducing the alkaline environment surrounding the CDs. The dendrimers act as buffer systems around the CDs, helping maintain and even enhance their emissive properties.

The effect of ionic strength on the fluorescence intensity of CDs and G4-G6 CDs@PAMAM nanohybrids was also studied using NaCl solutions at different concentrations (Figure S12 in the Supporting Information). The used salt concentrations varied between 0 and 200 mM with 20 mM increments. The results indicated good stability in the emission of CDs and G4-G6 CDs@PAMAM nanohybrids at all salt concentrations. CDs fluorescence only drops 30% at 200 mM NaCl, and, as for the G4-G6 CDs@PAMAM nanohybrids, fluorescence drops between 10 and 20% at 200 mM NaCl, depending on dendrimer generation. Results were very similar when changing the Na^+ cation for the K^+ one (Figure S13 in the Supporting Information). So, it seems that PAMAM dendrimers also protect CDs from quenching at high salt concentrations. This finding is relevant since it is known that the ionic strength can significantly vary in the physiological environment.[73]

3.4. Cell Viability Studies with the CDs@PAMAM Nanohybrids. The effect of CDs, G4-G6 PAMAM-NH_2 dendrimers, and G4-G6 CDs@PAMAM nanohybrids on cell viability was studied *in vitro* using HEK 293T cells and the concentrations of 1, 10, 25, 50, and 100 μg mL^{-1} for an exposition time of 48 h (Figure 7). A metabolic activity assay (resazurin reduction assay) was used as an indirect measure of cell viability. In this assay, resazurin is converted to resorufin in the mitochondria of viable cells. Then, resorufin fluorescence intensity is assumed as being directly proportional to the number of viable cells in culture. Results are expressed as a percentage of the average value obtained for non-exposed cells (control). Importantly, CDs and G4-G6 CDs@PAMAM nanohybrids' fluorescence does not interfere with this assay since these absorb until a maximum of 500 nm, and the fluorescence over 550 nm is inconsequential.

The results show that CDs are of low cytotoxicity toward HEK 293T cells, with cell viability only dropping to 80% at 100 μg mL^{-1}. Similar to what was observed by Ghosh *et al.*[57] regarding G1-G3 CDs@PAMAM nanohybrids, the toxicity of our G4-G6 CDs@PAMAM nanohybrids and that of the G4-G6 PAMAM-NH_2 dendrimers was dependent on dendrimer generation. Results showed that the G4 and G5 CDs@PAMAM nanohybrids were less toxic than the respective G4 and G5 PAMAM dendrimers. For instance, the G4 CDs@PAMAM nanohybrid presented cell viability of 76% at 100 μg/mL, whereas that for G4 PAMAM-NH_2 was 25% for the same

https://doi.org/10.1021/acs.biomac.1c00232
Biomacromolecules 2021, 22, 2436−2450

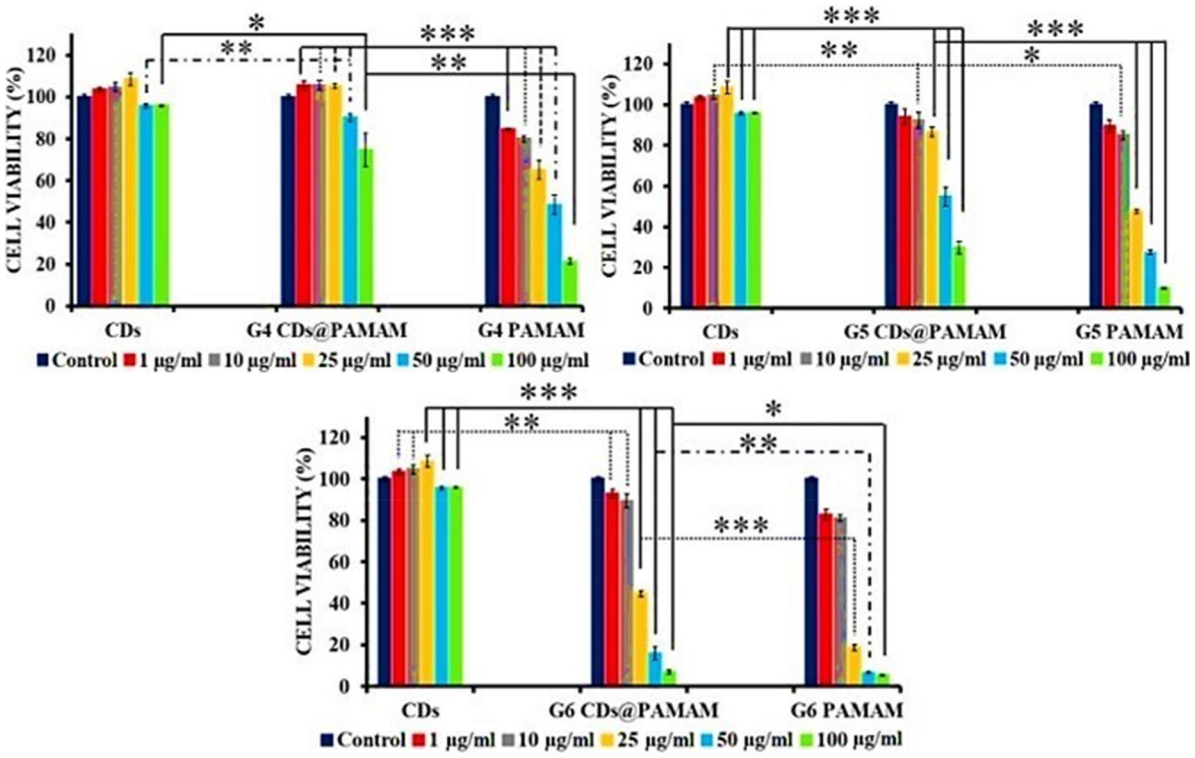

Figure 7. Effect of CDs, G4-G6 PAMAM-NH_2 dendrimers, and G4-G6 CDs@PAMAM nanohybrids on HEK 293T cell viability by the resazurin reduction assay. Results are expressed as a percentage of the average value obtained for non-exposed cells (control). The results obtained are mean ± StDev (n = 3), and statistical significance is represented as *(p < 0.05), **(p < 0.01), and ***(p < 0.001); comparisons were made between CDs vs G4-G6 CDs@PAMAM nanohybrids and G4-G6 CDs@PAMAM nanohybrids vs G4-G6 PAMAM-NH_2 dendrimers.

concentration. The same behavior was also observed for G5 CDs@PAMAM nanohybrids. In summary, although less cytocompatible than CDs alone, the nanohybrids formed by the self-assembly of CDs with PAMAM dendrimers led to more favorable dose-effect profiles than pristine dendrimers.

3.5. Cellular Internalization Studies with the CDs@PAMAM Nanohybrids. In view of their biological applications, studies were made to evaluate CDs@PAMAM nanohybrids ability to be internalized by cells, and results were compared with those obtained using CDs alone. These assays were based on both nanomaterials fluorescence properties and were performed using HEK 293T cells after an incubation time of 24 h. The extent of CDs or G4-G6 CDs@PAMAM nanohybrids cellular uptake was determined by flow cytometry, whereas fluorescence microscopy was used to confirm the possibility of using these nanomaterials as bioimaging agents, that is, to make sure they can effectively be visualized in a biological environment.

The flow cytometry studies were carried out using a fixed number of cells (10000), and the fluorescence was detected using an excitation laser of 405 nm and two detection channels, 530 nm (AmCyan) and 615 nm (Qdot 605). Figure 8 shows the mean fluorescence intensity detected by flow cytometry for the control (no exposed cells) and for cells exposed to solutions of CDs or G4-G6 CDs@PAMAM nanohybrids. The fluorescence emission detected in the control is due to the auto-fluorescence of cells as they possess organic molecules that also emit in the green and red region of the visible spectra. As for the CDs, for both green and red emissions, the detected fluorescence intensity was slightly higher than for the control but significantly lower than for the G4-G6 CDs@PAMAM nanohybrids. These results indicate a less effective accumulation of CDs inside HEK 293T cells due to their anionic surface that does not favor cell internalization. On the contrary, nanohybrids cell uptake was likely favored by their positive charge. Since, at neutral pH, the dendrimers presence in the nanohybrids induced quenching in the CDs fluorescence (as seen in Section 3.3), the extent of nanohybrid cell uptake should be even higher than that reflected in the results shown in Figure 8. Regarding the G4-G6 CDs@PAMAM nanohybrids, it seems that there is a dendrimer generation-dependent internalization, which a slight increase in the ζ-potential can explain, but not only, once cell uptake may depend on several other factors, like, for example, nanohybrid

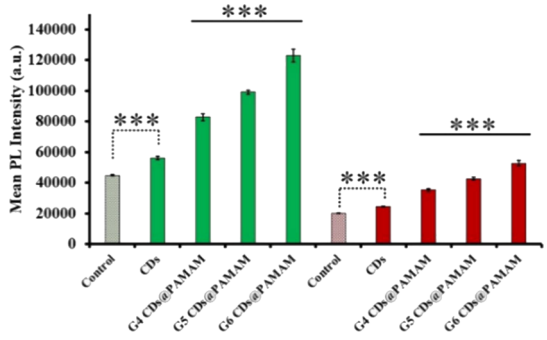

Figure 8. Mean fluorescence intensity of CDs and G4-G6 CDs@PAMAM hybrids was detected using flow cytometry after 24 h of incubation time. Green and red bars were obtained with the detection channel AmCyan (530 nm) and Qdot 605 (615 nm), respectively. The data are represented as mean ± StDev (n = 3), and the statistical significance as ***(p < 0.001); the comparisons were made against the control and CDs.

https://doi.org/10.1021/acs.biomac.1c00232
Biomacromolecules 2021, 22, 2436−2450

morphology.[74] Finally, it should be noticed that green fluorescence intensities are higher than red ones since, for the excitation wavelength used (405 nm), fluorescence is higher at 530 nm than at 615 nm (see Figure 1c).

As for fluorescence microscopy, the samples with cells exposed to CDs and G4-G6 CDs@PAMAM nanohybrids were excited with a blue and green light, which resulted in green and red emissions, respectively (Figure 9). As expected, samples

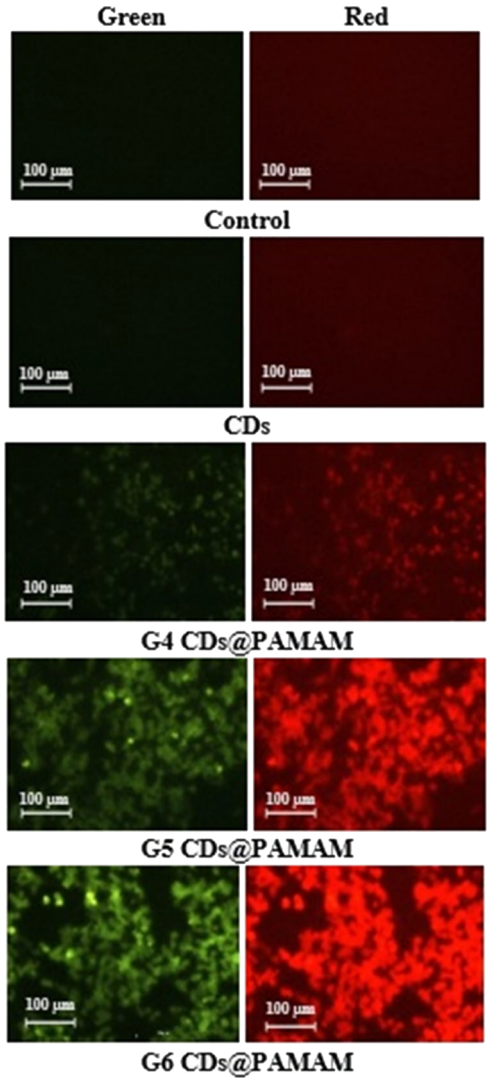

Figure 9. Fluorescence microscopy images of HEK 293T cells after 24 h of exposure to 300 μg/mL solutions of CDs and G4-G6 CDs@PAMAM nanohybrids. Excitation was produced with blue and green light for the observed green and red emission, respectively.

with non-exposed HEK 293T cells (control) emitted weak fluorescence, and they were not observed by fluorescence microscopy. In the case of samples exposed to carbon dots, as their cellular internalization was difficult due to their anionic surface, fluorescence signals were missing too.

Concerning the samples exposed to G4-G6 CDs@PAMAM nanohybrids, both green and red fluorescence were observed when excitation was done at two different wavelengths. For the nanohybrids, there was an evident increase in fluorescence with dendrimer generation, confirming the quantitative results of flow cytometry, that is, the cell uptake follows the trend G4 CDs@PAMAM nanohybrid < G5 CDs@PAMAM nanohybrid < G6 CDs@PAMAM nanohybrid.

Thus, our results indicate that the produced fluorescent nanohybrids are suitable for bioimaging applications and that their cellular internalization can even be tuned by playing with the PAMAM dendrimer generation.

3.6. DNA Condensation. As our objective was to test the nanohybrids as gene delivery vehicles, their capacity to condense plasmid DNA (pDNA) forming electrostatic complexes (hybridplexes) was studied and compared with those of CDs and G4-G6 PAMAM-NH_2 dendrimers. Experiments were done using the PicoGreen assay and CD/pDNA, nanohybrid/pDNA, or dendrimer/pDNA (w/w) ratios of 1, 2, 5, 10, 20, 50, and 100 in complex preparation (Figure 10). The PicoGreen assay can be applied to evaluate the nanomaterials capacity to condense DNA by using a fluorochrome with a maximum fluorescence emission when bonded to DNA.

If the fluorescence intensity decreases, it means that PicoGreen fluorochrome is not bonded to DNA and that the nanomaterial understudy is condensing it.[75] Importantly, even if interferences between the CDs fluorescence and the PicoGreen assay could occur as CDs also emit in the blue region, the used quantity of CDs or G4-G6 CDs@PAMAM nanohybrids was small enough for that to happen. The analysis of the results in Figure 10 shows that the pristine CDs cannot condense DNA, probably due to their anionic surface and the establishment of repulsion forces between them and the anionic pDNA molecule. For both the pristine dendrimers and the nanohybrids, DNA condensation was successful already at dendrimer/pDNA or nanohybrid/pDNA (w/w) ratios of 2, achieving full condensation for ratios ≥10. As for the pristine dendrimers, the higher generations were more efficient in the process, which can be explained by the higher number of amine groups present at their surface and protonated at neutral pH. In nanohybrids' case, pDNA condensation was also generation-dependent, with G4 and G5-based nanohybrids being better condensation agents. This dendrimer generation dependency of the nanohybrids is in line with the findings reported by Ghosh *et al.*[57] using lower generations of PAMAM dendrimers (G1-G3) in the nanohybrid formulation.

The PicoGreen assay reveals the extension of pDNA condensation but does not give information concerning the size of the formed complexes. The G4-G6 CDs@PAMAM/pDNA complexes at a ratio of 20 were then analyzed by TEM (Figure 11). The results show spherical morphologies for the hybridplexes, which are well separated from each other. The G4-based nanohybrids formed DNA complexes having an average diameter of 164 nm that show some polydispersity. In turn, the G6-based nanohybrids were less polydisperse and presented an average diameter of 43 nm. As for the G5-based nanohybrids, their condensates with pDNA were much smaller, having an average diameter of 21 nm. In this case, the hybridplexes were almost monodisperse, which makes them more suitable for pharmaceutical applications. So, overall, considering the results from the PicoGreen assay and TEM, one can conclude that the G5-based nanohybrids not only lead to a high pDNA condensation but also to the formation of nanohybrid/pDNA complexes that are small and uniform, possibly more capable of being internalized by cells and more prone to deliver DNA efficiently.

3.7. Transfection Studies. Transfection studies were conducted in HEK 293T cells using CD/pDNA, hybridplex (nanohybrid/pDNA), or dendrimer/pDNA ratios (w/w) of 2,

https://doi.org/10.1021/acs.biomac.1c00232
Biomacromolecules 2021, 22, 2436−2450

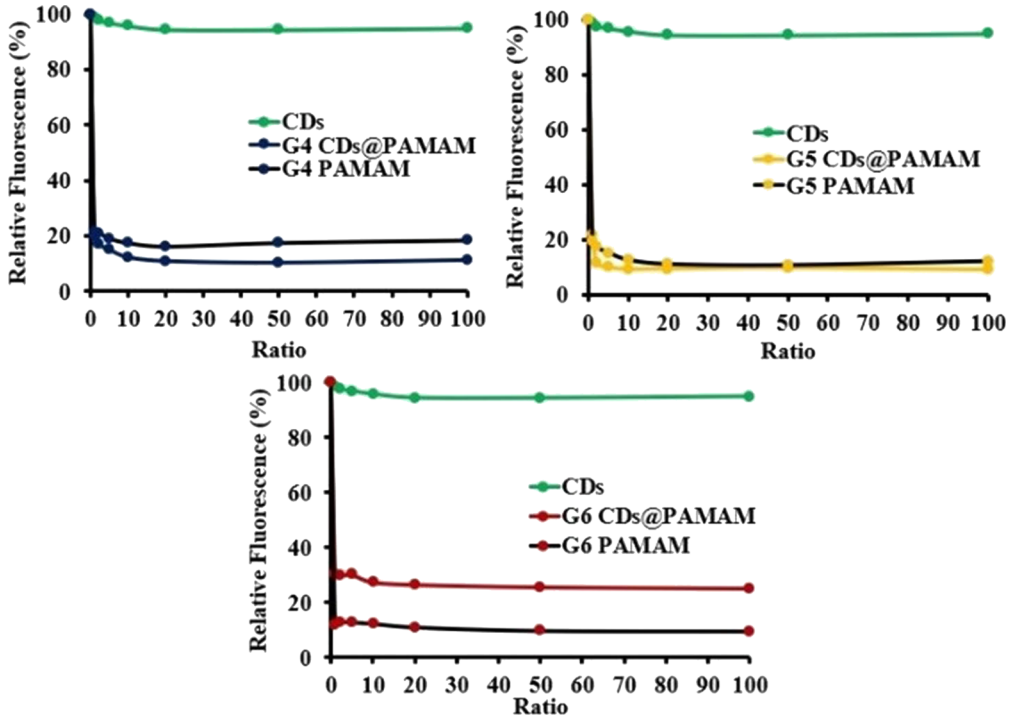

Figure 10. pDNA condensation using the PicoGreen assay. Experiments were done for CD/pDNA, nanohybrid/pDNA, or G4-G6 PAMAM/pDNA (w/w) ratios of 1, 2, 5, 10, 20, 50, and 100.

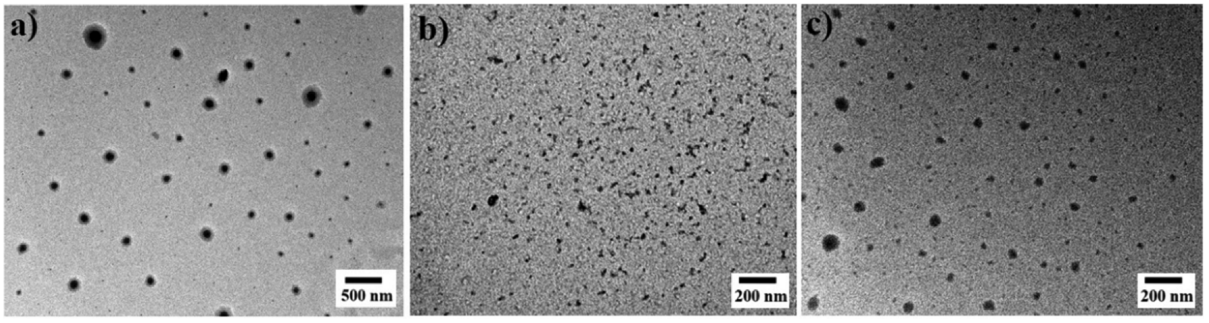

Figure 11. TEM micrographs of (a) G4 CDs@PAMAM/pDNA, (b) G5 CDs@PAMAM/pDNA, and (c) G6 CDs@PAMAM/pDNA condensates.

10, and 20 in complex preparation. The cells were exposed to the complexes, and results were accessed after 48 h. The pDNA used in the assays carried the green fluorescence protein (GFP) and the luciferase (Luc) reporter genes. Whereas GFP expression was used for a qualitative evaluation of transfection by fluorescence microscopy (cells expressing GFP appear with green color), luciferase activity (normalized in relation to the protein content) was determined for obtaining quantitative data of the process. Moreover, the protein content was used as an indirect measure of cell viability after exposure to the CD/pDNA, nanohybrid/pDNA, or dendrimer/pDNA complexes. Regarding the complexes effect on cell viability (Figure S14 in the Supporting Information), those prepared with CDs or G4 CDs@PAMAM nanohybrids were not more toxic than using naked pDNA. For all other cases except hybridplex or dendrimer/pDNA ratios of 2, cytotoxic effects were observed with increasing nanohybrid/pDNA or dendrimer/pDNA ratio values. In particular, the complexes formed with G6 CDs@PAMAM nanohybrids achieved high cytotoxicity levels at a nanohybrid/pDNA ratio of 10 and 20, for which reductions in cell viability of about 53% and 74% (in relation to naked pDNA) were respectively attained.

This cytotoxic effect was softer for the complexes prepared with G5 CDs@PAMAM nanohybrids.

As for fluorescence microscopy results, Figure 12 clearly shows that the CDs alone could not act as gene delivery agents since no GFP was expressed by cells (no green cells were observed). This finding was expected as CDs could not compact pDNA due to the presence of carboxylic acid groups on the surface. However, both the nanohybrids and the dendrimers were able to assume that role at all nanohybrid/pDNA or dendrimer/pDNA ratios tested. A clear observation from the experiments was that the transfection level always increased with an increase in these ratios. Also, out of the three types of nanohybrids, G5- and G6-based ones presented the best transfection performance, as evidenced by the higher extent of cells expressing GFP.

Figure 13 presents the results for normalized luciferase activity. Here, we can observe that the transfection efficiency achieved using CDs alone as gene delivery agents was residual. Additionally, and in general terms, the complexes prepared

https://doi.org/10.1021/acs.biomac.1c00232
Biomacromolecules 2021, 22, 2436−2450

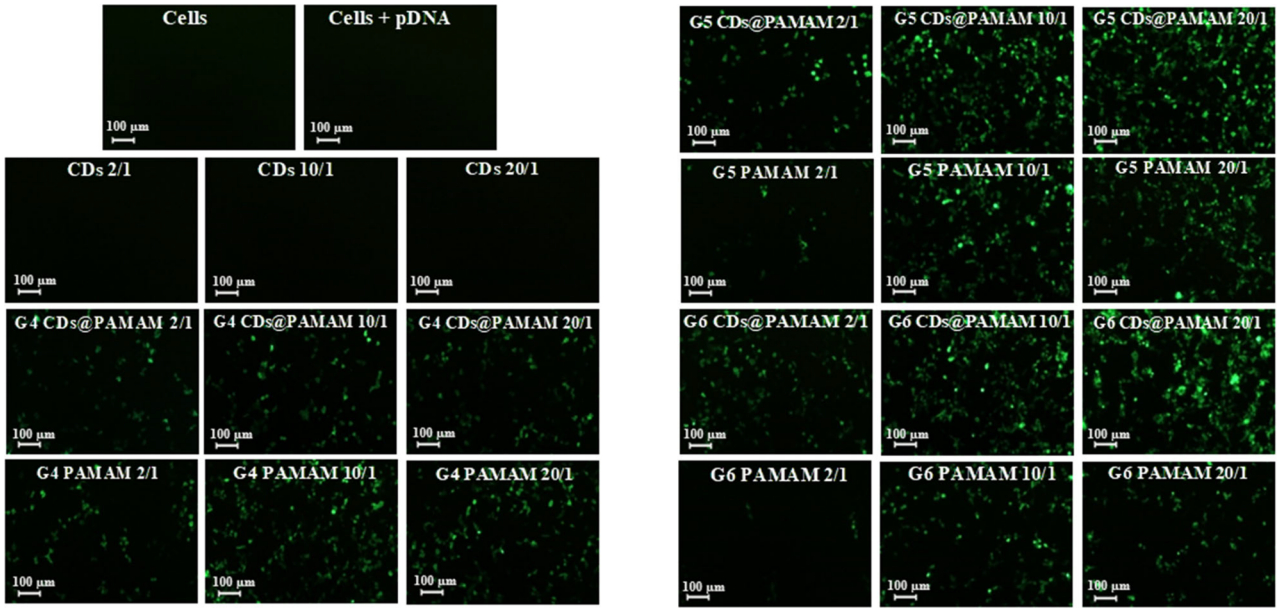

Figure 12. Fluorescence microscopy images showing GFP expression in HEK 293T cells 48 h post-transfection. Experiments were done for increasing CD/pDNA, nanohybrid/pDNA or dendrimer/pDNA ratios (w/w) (2, 10, and 20). Control experiments were performed using non-exposed cells and cells only exposed to free pDNA.

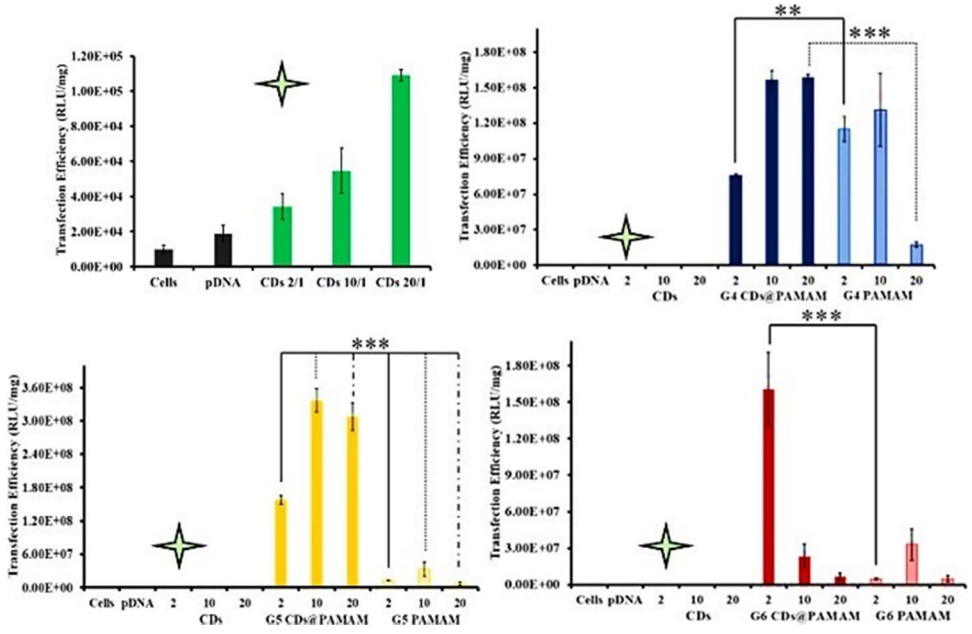

Figure 13. Transfection efficiency expressed as normalized luciferase activity (48 h post-transfection). Transfection assays were done at CD/pDNA, nanohybrid/pDNA, or dendrimer/pDNA ratios (w/w) of 2, 10, and 20 in HEK 293T cells. RLU/mg means relative light units per mg of total protein. The results obtained are mean ± StDev (n = 3), and statistical significance is represented as **(p < 0.01) and ***(p < 0.001), and comparisons were made between the G4-G6 CDs@PAMAM hybrids and the respective G4-G6 PAMAM dendrimers at the same ratios.

with the nanohybrids were much more efficient in gene delivery than those that used the pristine dendrimers (except for the G4 PAMAM-NH_2 dendrimer at dendrimer/pDNA ratios of 2 and 10). In fact, the G5 CDs@PAMAM nanohybrids were shown to be the best systems for the envisaged objective, with transfection efficiencies surpassing all other materials under study. Likely, the excellent performance of G5 CDs@PAMAM nanohybrids as gene delivery agents is associated with their excellent capacity to condense pDNA, forming small and monodispersed complexes.

4. CONCLUSIONS

In summary, anionic fluorescent CDs with an apparent round shape and the average size of 4 nm emitting in the blue, green, or orange/red region of the visible spectra were successfully synthesized using ascorbic acid and mild and original reaction conditions. For the first time, stable fluorescent CDs were self-assembled with PAMAM dendrimers generation 4 to 6 (G4-G6) to form G4-G6 CDs@PAMAM nanohybrids without compromising the physical and chemical characteristics of the pristine CDs and PAMAM dendrimers. Like the others presented below, this aspect is important considering the

https://doi.org/10.1021/acs.biomac.1c00232
Biomacromolecules 2021, 22, 2436−2450

design and preparation of dendrimers/CDs nanohybrids for biomedical applications.

Unlike the new isolated CDs, the fluorescence emitted by these nanohybrids remains high at pH values that are far from neutrality, which is due to the presence of dendrimers in their composition and the buffering effect they exert on the global structure. The nanohybrids cytocompatibility was located between that of CDs (non-toxic in the range of concentrations tested) and pristine dendrimers. Notably, the nanohybrids were easily internalized by cells in culture (much better than CDs alone) and, in addition, be detected through fluorescence emission in different colors, depending on the excitation wavelength used.

Furthermore, the G4-G6 CDs@PAMAM nanohybrids could compact pDNA, forming a type of complexes, coined hybridplexes, acting as gene delivery agents with transfection capabilities that surpassed those of pristine dendrimers. In particular, the nanohybrids based on G5 PAMAM dendrimers were shown to form small and uniform complexes with pDNA that only had mild cytotoxicity and presented very high transfection efficiencies. Overall, and although this work opens the way for more in-depth studies (e.g., related to the mechanism of action and localization of CDs@PAMAM nanohybrids/hybridplexes), in this exploratory study, we demonstrated that the new G4-G6 CDs@PAMAM nanohybrids present the necessary properties to justify their exploration in nanomedicine, particularly for theranostics.

■ ASSOCIATED CONTENT

Supporting Information

The Supporting Information is available free of charge at https://pubs.acs.org/doi/10.1021/acs.biomac.1c00232.

Determination of quantum yields; complementary TEM image and figures of NMR, FTIR, DLS characterization, effect of pH on the fluorescence intensity, and ionic strength of CDs and G4-G6 CDs@PAMAM nanohybrids; and cell viability of the prepared compounds (PDF)

■ AUTHOR INFORMATION

Corresponding Author

João Rodrigues − *CQM - Centro de Química da Madeira, MMRG, Universidade da Madeira, 9020-105 Funchal, Portugal; School of Materials Science and Engineering/Center for Nano Energy Materials, Northwestern Polytechnical University, 710072 Xi'an, China;* orcid.org/0000-0003-4552-1953; Email: joaor@uma.pt

Authors

Ivo Martins − *CQM - Centro de Química da Madeira, MMRG, Universidade da Madeira, 9020-105 Funchal, Portugal;* orcid.org/0000-0003-3818-248X

Helena Tomás − *CQM - Centro de Química da Madeira, MMRG, Universidade da Madeira, 9020-105 Funchal, Portugal;* orcid.org/0000-0002-7856-2041

Fernando Lahoz − *Departamento de Física, IUdEA, Universidad de La Laguna, 38200 San Cristóbal de La Laguna, Tenerife, Spain*

Complete contact information is available at: https://pubs.acs.org/10.1021/acs.biomac.1c00232

Notes

The authors declare no competing financial interest.

■ ACKNOWLEDGMENTS

The authors acknowledge the support of FCT-Fundação para a Ciência e a Tecnologia (Base Fund UIDB/00674/2020 and Programmatic Fund UIDP/00674/2020, Portuguese Government Funds), ARDITI-Agência Regional para o Desenvolvimento da Investigação Tecnologia e Inovação through the project M1420-01-0145-FEDER-000005-CQM+ (Madeira 14-20 Program). I.J.M. acknowledges the support of project M1420-01-0145-FEDER-000005-CQM+ through the research scholarship ARDITI-CQM/2018/017-MDG. This work was also partially funded by Ministerio de Economía, Industria y Competitividad, Spain (Agencia Estatal de Investigación, AEI) and European Union-FEDER (PID2019-107335RA-I00 and PID2019-110430GB-C21).

■ REFERENCES

(1) Patel, S.; Nanda, R. Nanotechnology in Healthcare: Applications and Challenges. *Med. Chem.* **2015**, *05*, 528−533.

(2) Ibrahim, R. K.; Hayyan, M.; AlSaadi, M. A.; Hayyan, A.; Ibrahim, S. Environmental application of nanotechnology: air, soil, and water. *Environ. Sci. Pollut. Res.* **2016**, *23*, 13754−13788.

(3) Chong, K. P. Nanoscience and engineering in mechanics and materials. *J. Phys. Chem. Solids* **2004**, *65*, 1501−1506.

(4) Krystek, M.; Górski, M. Nanomaterials in Structural Engineering. In *New Uses of Micro and Nanomaterials*. Pagnola, M. R.; Vivero, J. U.; Marrugo, A. G. IntechOpen, 2018, DOI: 10.5772/intechopen.79995.

(5) Santos, C. S. C.; Gabriel, B.; Blanchy, M.; Menes, O.; García, D.; Blanco, M.; Arconada, N.; Neto, V. Industrial Applications of Nanoparticles − A Prospective Overview. *Mater. Today: Proc.* **2015**, *2*, 456−465.

(6) Santos, A.; Veiga, F.; Figueiras, A. Dendrimers as Pharmaceutical Excipients: Synthesis, Properties, Toxicity and Biomedical Applications. *Materials* **2020**, *13*, 65.

(7) Mignani, S.; Rodrigues, J.; Tomas, H.; Caminade, A.-M.; Laurent, R.; Shi, X.; Majoral, J.-P. Recent therapeutic applications of the theranostic principle with dendrimers in oncology. *Sci. China Mater.* **2018**, *61*, 1367−1386.

(8) Sajid, M. Dendrimers based sorbents: Promising materials for analytical extractions. *Trends Anal. Chem.* **2018**, *98*, 114−127.

(9) Wu, L.-p.; Ficker, M.; Christensen, J. B.; Trohopoulos, P. N.; Moghimi, S. M. Dendrimers in Medicine: Therapeutic Concepts and Pharmaceutical Challenges. *Bioconjugate Chem.* **2015**, *26*, 1198−1211.

(10) Abbasi, E.; Aval, S. F.; Akbarzadeh, A.; Milani, M.; Nasrabadi, T. H.; Joo, S. W.; Hanifehpour, Y.; Nejati-Koshki, K.; Pashaei-Asl, R. Dendrimers: synthesis, applications, and properties. *Nanoscale Res. Lett.* **2014**, *9*, 247.

(11) Astruc, D.; Rapakousiou, A.; Wang, Y.; Djeda, R.; Diallo, A.; Ruiz, J.; Ornelas, C. Review: Mixed-valent metallodendrimers: design and functions. *J. Coord. Chem.* **2014**, *67*, 3809−3821.

(12) Roy, R.; Shiao, T. C.; Rittenhouse-Olson, K. Glycodendrimers: versatile tools for nanotechnology. *Braz. J. Pharm. Sci.* **2013**, *49*, 85−108.

(13) Myers, V. S.; Weir, M. G.; Carino, E. V.; Yancey, D. F.; Pande, S.; Crooks, R. M. Dendrimer-encapsulated nanoparticles: New synthetic and characterization methods and catalytic applications. *Chem. Sci.* **2011**, *2*, 1632−1646.

(14) Jiménez, J. L.; Pion, M.; Javier de la Mata, F.; Gomez, R.; Muñoz, E.; Leal, M.; Muñoz-Fernandez, M. A. Dendrimers as topical microbicides with activity against HIV. *New J. Chem.* **2012**, *36*, 299−309.

(15) Devadoss, C.; Bharathi, P.; Moore, J. S. Energy Transfer in Dendritic Macromolecules: Molecular Size Effects and the Role of an Energy Gradient. *J. Am. Chem. Soc.* **1996**, *118*, 9635−9644.

(16) Li, J.; Shen, M.; Shi, X. Poly(amidoamine) Dendrimer-Gold Nanohybrids in Cancer Gene Therapy: A Concise Overview. *ACS Appl. Bio Mater.* **2020**, *3*, 5590−5605.
(17) Rabiee, N.; Ahmadvand, S.; Ahmadi, S.; Fatahi, Y.; Dinarvand, R.; Bagherzadeh, M.; Rabiee, M.; Tahriri, M.; Tayebi, L.; Hamblin, M. R. Carbosilane dendrimers: Drug and gene delivery applications. *J. Drug Deliv. Sci. Technol.* **2020**, *59*, 101879.
(18) Mignani, S.; Rodrigues, J.; Tomas, H.; Roy, R.; Shi, X.; Majoral, J.-P. Bench-to-bedside translation of dendrimers: Reality or utopia? A concise analysis. *Adv. Drug Delivery Rev.* **2018**, *136-137*, 73−81.
(19) Santos, S. D.; Xavier, M.; Leite, D. M.; Moreira, D. A.; Custódio, B.; Torrado, M.; Castro, R.; Leiro, V.; Rodrigues, J.; Tomás, H.; Pêgo, A. P. PAMAM dendrimers: blood-brain barrier transport and neuronal uptake after focal brain ischemia. *J. Controlled Release* **2018**, *291*, 65−79.
(20) Chen, L.; Li, J.; Fan, Y.; Qiu, J.; Cao, L.; Laurent, R.; Mignani, S.; Caminade, A.-M.; Majoral, J.-P.; Shi, X. Revisiting Cationic Phosphorus Dendrimers as a Non-viral Vector for Optimized Gene Delivery Toward Cancer Therapy Applications. *Biomacromolecules* **2020**, *21*, 2502−2511.
(21) Maciel, D.; Guerrero-Beltrán, C.; Ceña-Diez, R.; Tomás, H.; Muñoz-Fernández, M. Á.; Rodrigues, J. New anionic poly-(alkylideneamine) dendrimers as microbicide agents against HIV-1 infection. *Nanoscale* **2019**, *11*, 9679−9690.
(22) Restani, R. B.; Morgado, P. I.; Ribeiro, M. P.; Correia, I. J.; Aguiar-Ricardo, A.; Bonifácio, V. D. B. Biocompatible Polyurea Dendrimers with pH-Dependent Fluorescence. *Angew. Chem., Int. Ed.* **2012**, *51*, 5162−5165.
(23) Vögtle, F.; Richardt, G.; Werner, N. *Dendrimer Chemistry: Concepts, Syntheses, Properties, Applications*. Wiley-VCH Verlag GmbH & Co. KGaA, Weinheim. 2009, 354.
(24) Tomalia, D. A.; Baker, H.; Dewald, J.; Hall, M.; Kallos, G.; Martin, S.; Roeck, J.; Ryder, J.; Smith, P. A New Class of Polymers: Starburst-Dendritic Macromolecules. *Polym. J.* **1985**, *17*, 117−132.
(25) Esfand, R.; Tomalia, D. A. Poly(amidoamine) (PAMAM) dendrimers: from biomimicry to drug delivery and biomedical applications. *Drug Discovery Today* **2001**, *6*, 427−436.
(26) Contin, M.; Garcia, C.; Dobrecky, C.; Lucangioli, S.; D'Accorso, N. Advances in drug delivery, gene delivery and therapeutic agents based on dendritic materials. *Future Med. Chem.* **2019**, *11*, 1791−1810.
(27) de Araújo, R. V.; da Silva Santos, S.; Ferreira, E. I.; Giarolla, J. New Advances in General Biomedical Applications of PAMAM Dendrimers. *Molecules* **2018**, *23*, 2849.
(28) Gouveia, M.; Figueira, J.; Jardim, M.; Castro, R.; Tomás, H.; Rissanen, K.; Rodrigues, J. Poly(alkylidenimine) Dendrimers Functionalized with the Organometallic Moiety $[Ru(\eta^5\text{-}C_5H_5)\text{-}(PPh_3)_2]^+$ as Promising Drugs Against *Cisplatin*-Resistant Cancer Cells and Human Mesenchymal Stem Cells. *Molecules* **2018**, *23*, 1471.
(29) Mignani, S.; Rodrigues, J.; Tomas, H.; Zablocka, M.; Shi, X.; Caminade, A.-M.; Majoral, J.-P. Dendrimers in combination with natural products and analogues as anti-cancer agents. *Chem. Soc. Rev.* **2018**, *47*, 514−532.
(30) Ramalingam, K.; Castro, R.; Pires, P.; Shi, X.; Rodrigues, J.; Xiao, S.; Tomás, H. Gene delivery using dendrimer/pDNA complexes immobilized in electrospun fibers using the Layer-by-Layer technique. *RSC Adv.* **2016**, *6*, 97116−97128.
(31) Xiao, S.; Castro, R.; Rodrigues, J.; Shi, X.; Tomás, H. PAMAM Dendrimer/pDNA Functionalized-Magnetic Iron Oxide Nanoparticles for Gene Delivery. *J. Biomed. Nanotechnol.* **2015**, *11*, 1370−1384.
(32) Gonçalves, M.; Maciel, D.; Capelo, D.; Xiao, S.; Sun, W.; Shi, X.; Rodrigues, J.; Tomás, H.; Li, Y. Dendrimer-Assisted Formation of Fluorescent Nanogels for Drug Delivery and Intracellular Imaging. *Biomacromolecules* **2014**, *15*, 492−499.
(33) Santos, J. L.; Oliveira, H.; Pandita, D.; Rodrigues, J.; Pâgo, A. P.; Granja, P. L.; Tomás, H. Functionalization of poly(amidoamine) dendrimers with hydrophobic chains for improved gene delivery in mesenchymal stem cells. *J. Controlled Release* **2010**, *144*, 55−64.
(34) Ainalem, M.-L.; Nylander, T. DNA condensation using cationic dendrimers—morphology and supramolecular structure of formed aggregates. *Soft Matter* **2011**, *7*, 4577−4594.
(35) Janaszewska, A.; Lazniewska, J.; Trzepiński, P.; Marcinkowska, M.; Klajnert-Maculewicz, B. Cytotoxicity of Dendrimers. *Biomolecules* **2019**, *9*, 330−353.
(36) Bodewein, L.; Schmelter, F.; Di Fiore, S.; Hollert, H.; Fischer, R.; Fenske, M. Differences in toxicity of anionic and cationic PAMAM and PPI dendrimers in zebrafish embryos and cancer cell lines. *Toxicol. Appl. Pharmacol.* **2016**, *305*, 83−92.
(37) Camacho, C. S.; Urgellés, M.; Tomás, H.; Lahoz, F.; Rodrigues, J. New insights into the blue intrinsic fluorescence of oxidized PAMAM dendrimers considering their use as bionanomaterials. *J. Mater. Chem. B* **2020**, *8*, 10314−10326.
(38) Xu, X.; Ray, R.; Gu, Y.; Ploehn, H. J.; Gearheart, L.; Raker, K.; Scrivens, W. A. Electrophoretic Analysis and Purification of Fluorescent Single-Walled Carbon Nanotube Fragments. *J. Am. Chem. Soc.* **2004**, *126*, 12736−12737.
(39) Cayuela, A.; Soriano, M. L.; Carrillo-Carrión, C.; Valcárcel, M. Semiconductor and carbon-based fluorescent nanodots: the need for consistency. *Chem. Commun.* **2016**, *52*, 1311−1326.
(40) Wang, Y.; Hu, A. Carbon quantum dots: synthesis, properties and applications. *J. Mater. Chem. C* **2014**, *2*, 6921−6939.
(41) Cao, L.; Wang, X.; Meziani, M. J.; Lu, F.; Wang, H.; Luo, P. G.; Lin, Y.; Haruff, B. A.; Veca, L. M.; Murray, D.; Xie, S.-Y.; Sun, Y.-P. Carbon Dots for Multiphoton Bioimaging. *J. Am. Chem. Soc.* **2007**, *129*, 11318−11319.
(42) Zhu, S.; Meng, Q.; Wang, L.; Zhang, J.; Song, Y.; Jin, H.; Zhang, K.; Sun, H.; Wang, H.; Yang, B. Highly Photoluminescent Carbon Dots for Multicolor Patterning, Sensors, and Bioimaging. *Am. Ethnol.* **2013**, *52*, 3953−3957.
(43) Molaei, M. F. Carbon quantum dots and their biomedical and therapeutic applications: a review. *RSC Adv.* **2019**, *9*, 6460−6481.
(44) Mirtchev, P.; Henderson, E. J.; Soheilnia, N.; Yip, C. M.; Ozin, G. A. Solution phase synthesis of carbon quantum dots as sensitizers for nanocrystalline TiO_2 solar cells. *J. Mater. Chem.* **2012**, *22*, 1265−1269.
(45) Qu, K.; Wang, J.; Ren, J.; Qu, X. Carbon Dots Prepared by Hydrothermal Treatment of Dopamine as an Effective Fluorescent Sensing Platform for the Label-Free Detection of Iron(III) Ions and Dopamine. *Chem. − Eur. J.* **2013**, *19*, 7243−7249.
(46) Yu, H.; Zhao, Y.; Zhou, C.; Shang, L.; Peng, Y.; Cao, Y.; Wu, L.-Z.; Tung, C.-H.; Zhang, T. Carbon quantum dots/TiO_2 composites for efficient photocatalytic hydrogen evolution. *J. Mater. Chem. A* **2014**, *2*, 3344−3351.
(47) Dou, Q.; Fang, X.; Jiang, S.; Chee, P. L.; Lee, T.-C.; Loh, X. J. Multi-functional fluorescent carbon dots with antibacterial and gene delivery properties. *RSC Adv.* **2015**, *5*, 46817−46822.
(48) Kim, S.; Choi, Y.; Park, G.; Won, C.; Park, Y.-J.; Lee, Y.; Kim, B.-S.; Min, D.-H. Highly efficient gene silencing and bioimaging based on fluorescent carbon dots *in vitro* and *in vivo*. *Nano Res.* **2017**, *10*, 503−519.
(49) Wang, H.-J.; Zhang, J.; Liu, Y.-H.; Luo, T.-Y.; He, X.; Yu, X.-Q. Hyaluronic acid-based carbon dots for efficient gene delivery and cell imaging. *RSC Adv.* **2017**, *7*, 15613−15624.
(50) Havrdova, M.; Hola, K.; Skopalik, J.; Tomankova, K.; Petr, M.; Cepe, K.; Polakova, K.; Tucek, J.; Bourlinos, A. B.; Zboril, R. Toxicity of carbon dots − Effect of surface functionalization on the cell viability, reactive oxygen species generation and cell cycle. *Carbon* **2016**, *99*, 238−248.
(51) Ngu-Schwemlein, M.; Chin, S. F.; Hileman, R.; Drozdowski, C.; Upchurch, C.; Hargrove, A. Carbon nanodots as molecular scaffolds for development of antimicrobial agents. *Bioorg. Med. Chem. Lett.* **2016**, *26*, 1745−1749.
(52) Zong, J.; Yang, X.; Trinchi, A.; Hardin, S.; Cole, I.; Zhu, Y.; Li, C.; Muster, T.; Wei, G. Photoluminescence enhancement of carbon dots by gold nanoparticles conjugated *via* PAMAM dendrimers. *Nanoscale* **2013**, *5*, 11200−11206.

https://doi.org/10.1021/acs.biomac.1c00232
Biomacromolecules 2021, 22, 2436−2450

(53) Campos, B. B.; Oliva, M. M.; Contreras-Cáceres, R.; Rodriguez-Castellón, E.; Jimenéz-Jimenéz, J.; Esteves da Silva, J. C. G.; Algarra, M. Carbon dots on based folic acid coated with PAMAM dendrimer as platform for Pt(IV) detection. *J. Colloid Interface Sci.* **2016**, *465*, 165−173.
(54) Lin, T. N.; Inciong, M. R.; Santiago, S. R.; Kao, C. W.; Shu, G. W.; Yuan, C. T.; Shen, J. L.; Yeh, J. M.; Chen-Yang, Y. W. Electron injection from graphene quantum dots to poly(amido amine) dendrimers. *Appl. Phys. Lett.* **2016**, *108*, 161904.
(55) Li, D.; Fan, Y.; Shen, M.; Bányai, I.; Shi, X. Design of dual drug-loaded dendrimer/carbon dot nanohybrids for fluorescence imaging and enhanced chemotherapy of cancer cells. *J. Mater. Chem. B* **2019**, *7*, 277−285.
(56) Bhatnagar, D.; Kaur, I.; Kumar, A. Ultrasensitive cardiac troponin I antibody based nanohybrid sensor for rapid detection of human heart attack. *Int. J. Biol. Macromol.* **2017**, *95*, 505−510.
(57) Ghosh, S.; Ghosal, K.; Mohammad, S. A.; Sarkar, K. Dendrimer functionalized carbon quantum dot for selective detection of breast cancer and gene therapy. *Chem. Eng. J.* **2019**, *373*, 468−484.
(58) Guo, Y.; Shen, M.; Shi, X. Construction of Poly(amidoamine) Dendrimer/Carbon Dot Nanohybrids for Biomedical Applications. *Macromol. Biosci.* **2021**, *21*, 2100007.
(59) Hudde, T.; Rayner, S. A.; Comer, R. M.; Weber, M.; Isaacs, J. D.; Waldmann, H.; Larkin, D. F. P.; George, A. J. T. Activated polyamidoamine dendrimers, a non-viral vector for gene transfer to the corneal endothelium. *Gene Ther.* **1999**, *6*, 939−943.
(60) Dennig, J.; Duncan, E. Gene transfer into eukaryotic cells using activated polyamidoamine dendrimers. *Rev. Mol. Biotechnol.* **2002**, *90*, 339−347.
(61) Navarro, G.; Tros de Ilarduya, C. Activated and non-activated PAMAM dendrimers for gene delivery *in vitro* and *in vivo*. *Nanomed,:Nanotechnol., Biol., Med.* **2009**, *5*, 287−297.
(62) Cailotto, S.; Amadio, E.; Facchin, M.; Selva, M.; Pontoglio, E.; Rizzolio, F.; Riello, P.; Toffoli, G.; Benedetti, A.; Perosa, A. Carbon Dots from Sugars and Ascorbic Acid: Role of the Precursors on Morphology, Properties, Toxicity, and Drug Uptake. *ACS Med. Chem. Lett.* **2018**, *9*, 832−837.
(63) Zhao, Z.; Zhang, J.; Wang, Y.; Chen, L.; Zhang, Y. Hydrothermal synthesis of fluorescent nitrogen-doped carbon quantum dots from ascorbic acid and valine for selective determination of picric acid in water samples. *Int. J. Environ. Anal. Chem.* **2016**, *96*, 1402−1413.
(64) Sugiarti, S.; Darmawan, N. Synthesis of Fluorescence Carbon Nanoparticles from Ascorbic Acid. *Indones. J. Chem.* **2015**, *15*, 141−145.
(65) Sajid, P. A.; Chetty, S. S.; Praneetha, S.; Murugan, A. V.; Kumar, Y.; Periyasamy, L. One-pot microwave-assisted *in situ* reduction of Ag^{+} and Au^{3+} ions by *Citrus limon* extract and their carbon-dots based nanohybrids: a potential nano-bioprobe for cancer cellular imaging. *RSC Adv.* **2016**, *6*, 103482−103490.
(66) Allen, M.W. *Measurement of Fluorescent Quantum Yields. Technical note: 52019*; Thermo Fischer Scientific: Madison, WI, USA, 2010
(67) Lakowicz, J. R., *Principles of fluorescence spectroscopy*; 3rd Ed.; Springer: New York, 2006; pp. 141−142.
(68) Kalytchuk, S.; Wang, Y.; Poláková, K.; Zbořil, R. Carbon Dot Fluorescence-Lifetime-Encoded Anti-Counterfeiting. *ACS Appl. Mater. Interfaces* **2018**, *10*, 29902−29908.
(69) Lecroy, G. E.; Messina, F.; Sciortino, A.; Bunker, C. E.; Wang, P.; Fernando, K. A. S.; Sun, Y.-P. Characteristic Excitation Wavelength Dependence of Fluorescence Emissions in Carbon "Quantum" Dots. *J. Phys. Chem. C* **2017**, *121*, 28180−28186.
(70) Shao, J.; Zhu, S.; Liu, H.; Song, Y.; Tao, S.; Yang, B. Full-Color Emission Polymer Carbon Dots with Quench-Resistant Solid-State Fluorescence. *Adv. Sci.* **2017**, *4*, 1700395.
(71) Pande, S.; Crooks, R. M. Analysis of Poly(amidoamine) Dendrimer Structure by UV−Vis Spectroscopy. *Langmuir* **2011**, *27*, 9609−9613.
(72) Jackson, C. L.; Chanzy, H. D.; Booy, F. P.; Drake, B. J.; Tomalia, D. A.; Bauer, B. J.; Amis, E. J. Visualization of Dendrimer Molecules by Transmission Electron Microscopy (TEM): Staining Methods and Cryo-TEM of Vitrified Solutions. *Macromolecules* **1998**, *31*, 6259−6265.
(73) Liu, B.; Poolman, B.; Boersma, A. J. Ionic Strength Sensing in Living Cells. *ACS Chem. Biol.* **2017**, *12*, 2510−2514.
(74) Gratton, S. E. A.; Ropp, P. A.; Pohlhaus, P. D.; Luft, J. C.; Madden, V. J.; Napier, M. E.; DeSimone, J. M. The effect of particle design on cellular internalization pathways. *Proc. Natl. Acad. Sci.* **2008**, *105*, 11613−11618.
(75) Nie, X.; Zhang, Z.; Wang, C.-H.; Fan, Y.-S.; Meng, Q.-Y.; You, Y.-Z. Interactions in DNA Condensation: An Important Factor for Improving the Efficacy of Gene Transfection. *Bioconjugate Chem.* **2019**, *30*, 284−292.

https://doi.org/10.1021/acs.biomac.1c00232
Biomacromolecules 2021, 22, 2436−2450